



**HAL**  
open science

## High-resolution infrared and subterahertz spectroscopy of the $v_2=1$ , $v_5=1$ , and $v_3=2$ levels of $^{13}\text{CH}_3^{35}\text{Cl}$

Florin Lucian Constantin, J. Demaison, L. Féjard, M. Litz, H. Bürger, P.  
Pracna

► **To cite this version:**

Florin Lucian Constantin, J. Demaison, L. Féjard, M. Litz, H. Bürger, et al.. High-resolution infrared and subterahertz spectroscopy of the  $v_2=1$ ,  $v_5=1$ , and  $v_3=2$  levels of  $^{13}\text{CH}_3^{35}\text{Cl}$ . *Journal of Molecular Spectroscopy*, 2007, 243 (2), pp.234-244. 10.1016/j.jms.2007.04.002 . hal-03335695

**HAL Id: hal-03335695**

**<https://hal.science/hal-03335695>**

Submitted on 23 Sep 2021

**HAL** is a multi-disciplinary open access archive for the deposit and dissemination of scientific research documents, whether they are published or not. The documents may come from teaching and research institutions in France or abroad, or from public or private research centers.

L'archive ouverte pluridisciplinaire **HAL**, est destinée au dépôt et à la diffusion de documents scientifiques de niveau recherche, publiés ou non, émanant des établissements d'enseignement et de recherche français ou étrangers, des laboratoires publics ou privés.

# ***High-resolution Infrared and Subterahertz Spectroscopy of the $\nu_2 = 1, \nu_5 = 1, \text{ and } \nu_3 = 2$ Levels of $^{13}\text{CH}_3\ ^{35}\text{Cl}$***

F.L. CONSTANTIN,<sup>1</sup> J. DEMAISON,<sup>1</sup> L. FÉJARD,<sup>2</sup> M. LITZ,<sup>2</sup>  
H. BÜRGER,<sup>2</sup> P. PRACNA,<sup>1,3 \*</sup>

<sup>1</sup> Laboratoire de Physique des Lasers, Atomes et Molécules, UMR CNRS 8523, Bât. P5,  
Université de Lille I, F-59655 Villeneuve d'Ascq Cedex, France

<sup>2</sup> FB C-Anorganische Chemie, Universität, D-42097 Wuppertal, Germany

<sup>3</sup> J. Heyrovský Institute of Physical Chemistry, Academy of Sciences of the Czech Republic,  
Dolejškova 3, 182 23 Prague 8, Czech Republic

## ***Abstract***

High-resolution Fourier-transform infrared spectra between 1235 and 1680  $\text{cm}^{-1}$  and subterahertz spectra between 250 and 630 GHz of monoisotopic  $^{13}\text{CH}_3\ ^{35}\text{Cl}$  have been recorded and analyzed simultaneously, with all Coriolis,  $\alpha$ -resonance, and  $l$ -type interactions in the polyad of the  $\nu_2 = 1, \nu_5 = 1, \text{ and } \nu_3 = 2$  levels taken into account. Several  $\alpha$ -resonances ( $\Delta k = \pm 2, \Delta l = \mp 1$ ) generating perturbation-allowed transitions have been assigned in the rovibrational spectra. These resonances enabled us to determine accurately and independently the ground state rotational and centrifugal distortion parameters  $A_0 = 5.205\,746\,9(55)\text{ cm}^{-1}$  and  $D_K^0 = 8.440\,4(84) \times 10^{-5}\text{ cm}^{-1}$ . Even  $H_K^0 = 8.527(39) \times 10^{-9}\text{ cm}^{-1}$ , which is, however, correlated to higher-order  $\alpha$ -resonance terms, was determined. With 51 upper state parameters varied, about 5800 rovibrational wavenumbers and more than 550 rotational frequencies pertaining to the excited vibrational states were fitted within their experimental accuracy.

## 1. Introduction

Because of its abundance and easy photodissociation, methyl chloride has been extensively studied by high-resolution spectroscopy as an important source of chlorine in the Earth's atmosphere. In this context the desirable accurate determination of the equilibrium structure and of the molecular force field requires the knowledge of rotational constants in excited fundamental levels of several isotopic species as well as of the Coriolis  $\zeta$  and centrifugal distortion constants. The present work that has been started recently using monoisotopic samples [1-2] is a contribution to a systematic reinvestigation of the less abundant species  $^{13}\text{CH}_3\ ^{35}\text{Cl}$  and  $^{13}\text{CH}_3\ ^{37}\text{Cl}$  (abbreviated here as 1335 and 1337). Previously, only low-resolution studies (0.2 - 0.3  $\text{cm}^{-1}$ ) of the methyl chloride species with  $^{13}\text{C}$  and chlorine in natural abundance were available [3], in which only the isotopic shifts of the  $\nu_2$  and  $\nu_3$  bands were discerned.

The studies of the 1335 and 1337 species were started by investigation of their vibrational ground states and the two lowest fundamental vibrational levels  $\nu_3 = 1$  and  $\nu_6 = 1$  by rotational spectroscopy in the terahertz and subterahertz wave range and by infrared Fourier-transform spectroscopy [1]. The ground state constants were determined from purely rotational frequencies merged with combination differences obtained from wavenumbers of the  $\nu_3$  and  $\nu_6$  bands. In addition to this, the axial constants  $A_0$  in both isotopic species were determined from perturbation-allowed (PA) transitions in the  $\nu_2$  and  $\nu_5$  bands assigned around a local crossing due to  $\Delta k = \pm 2, \Delta l = \mp 1$   $\alpha$ -resonance. The accuracy of the determination of  $A_0$  still remained influenced by the uncertainty of  $D_K^0$  which was taken from the harmonic force field of Black and Law [4]. Very recently, ground state rotational spectra of the 1235 and 1335 species have been reinvestigated in the region 76 – 282 GHz with the emphasis on the detailed description of hyperfine splittings and accurate determination of purely rotational (hyperfine-free) frequencies [5].

Independent studies of the species 1235 and 1237 which are those most abundant in natural methyl chloride were recently performed but with a different approach [6,7]. High-resolution FTIR spectra of similar quality as available in the present study and also based on monoisotopic material were used. The analyses reported in [6,7] were done by considering simultaneously all lower polyads up to 1800 and 2600  $\text{cm}^{-1}$ , respectively, and employing the tensorial method to reproduce the observed spectra with experimental uncertainty. The emphasis of these global fits was above all put on the consistency of corresponding molecular parameters for the different excited states involved. The present study, however, stresses, in a line-by-line type exploration,

in particular weak although most informative interactions exceeding the major avoided crossings mentioned in Refs. [1,6,7].

In detail the large isotopic shift of the  $\nu_3 = 2$  vibrational level in the heavier  $^{13}\text{C}$  isotopologues displaces the vibrational energy pattern of the polyad  $\nu_2 = 1$ ,  $\nu_5 = 1$ , and  $\nu_3 = 2$  with regard to the lighter  $^{12}\text{C}$  species. In correspondence the energies of the vibrational levels in the  $^{13}\text{C}$  species are altered such that several resonant crossings due to interactions with selection rules for nonvanishing Hamiltonian elements  $\Delta k = \pm 2$ ,  $\Delta \ell = \mp 1$  ( $\alpha$ -resonances) become observable. These interactions cause significant mixing of rovibrational wavefunctions and consequently induce series of perturbation-allowed transitions which span several  $\Delta K = 3$  intervals in the vibrational ground state. This enables one to determine accurately in addition to the rotational constant  $A_0$  also the quartic and sextic centrifugal distortion terms  $D_K^0$  and  $H_K^0$ . Here we present our results for 1335, while those obtained for the same polyad of 1337 were reported previously [2]. For this purpose we have analyzed simultaneously vibration-rotation wavenumbers of the three infrared bands  $\nu_2$ ,  $\nu_5$ , and  $2\nu_3$ , together with rotational data pertaining to the upper vibrational levels.

## 2. Experimental details

The synthesis of 1335, isotopic enrichment 99.4 %  $^{13}\text{C}$  and 99.32 %  $^{35}\text{Cl}$ , has been described previously [1]. Two different high-resolution Fourier transform spectra were recorded. The weaker one initially used is that denoted 35-4 in Ref. [1], obtained employing a cell of 28 cm pathlength and a pressure of 400 Pa. The resolution ( $1 / \text{maximum optical path difference}$ ) was  $2.7 \times 10^{-3} \text{ cm}^{-1}$ , precision about  $5 \times 10^{-5} \text{ cm}^{-1}$ , accuracy ca.  $5 \times 10^{-4} \text{ cm}^{-1}$ . The second spectrum measured using a White-type multipass cell adjusted to a path length of 9.6 m and a pressure of 200 Pa was about 17 times more intense than the weaker spectrum and served to reach higher rotational states, to search weak PA transitions, and to evaluate the  $2\nu_3$  band. This spectrum had the same resolution of  $2.7 \times 10^{-3} \text{ cm}^{-1}$ . It was also obtained with a Bruker 120 HR interferometer equipped with a Globar source, a  $\text{CaF}_2$  beam splitter and a  $4.2 \mu\text{m}$  low-pass filter. In total 960 scans were coadded and the spectrum extending from  $1235 - 1680 \text{ cm}^{-1}$  was calibrated by comparing wavenumbers with those of the weaker spectrum already described in [1]. The wavenumber precision of isolated lines is about  $2 \times 10^{-4} \text{ cm}^{-1}$ .

The subterahertz measurements performed in Lille were done with a backward-wave oscillator (BWO) spectrometer. We used Russian ISTOK backward-wave oscillators in the range 175-355 GHz and 505-615 GHz phase-locked on a harmonic of a microwave synthesizer referenced to the GPS frequency standard. We developed a computer-controlled frequency-multiplication chain allowing broadband scan of the BWO frequency that guarantees rigorous phase lock

accuracy at each experimental point. Radiation from the microwave synthesizer (HP 83711A) was frequency-multiplied and amplified by a Millitech active frequency multiplier (AMC-10-R000) covering the 75-110 GHz range with a power level greater than 4 dBm. The BWO radiation was focused with a parabolic mirror on a planar diode mixer (Virginia Diodes) and heterodyned with successive harmonics of the active frequency multiplier. The intermediate frequency signal at 320 MHz was filtered (with a bandwidth of 10 MHz) and amplified with a broadband low-noise amplifier, leading to a typical signal at more than 30 dB above noise recorded with a resolution bandwidth of 10 kHz. The comparison of the intermediate frequency signal with the 32<sup>nd</sup> harmonic of a radio frequency synthesizer (HP 3325B operating around 10 MHz) provides an error signal that drives the BWO current supply for phase locking purpose. The bandwidth of the correction loop is a few MHz. The BWO frequency can be precisely stepped over the molecular lines of interest by successively incrementing the HP 3325B synthesizer in the range 9.75-10.25 MHz and further the HP 83711A synthesizer. A watchdog-loop in the software guarantees the phase-lock status of the BWO at each step.

We used a frequency modulation detection technique (frequency-modulation of HP 3325B at 5 kHz with a modulation depth of 400 kHz) associated to a 2-f demodulation with a lock-in amplifier. The detector is a Queen Mary College liquid-helium cooled InSb bolometer. We used a stainless-steel circular absorption cell with 1.1 m length and 6 cm diameter. The measurements were done at room temperature and at a typical pressure of 4 Pa.

### ***3. General description of the IR spectra***

The general appearance of the studied infrared spectrum of 1335 in the region of the  $\nu_2$ ,  $\nu_5$ , and  $2\nu_3$  bands is very similar to that of the 1337 species (see Fig. 1). The two fundamental bands have their band origins within  $0.5 \text{ cm}^{-1}$  from those of the 1337 species and all their features concerning intensity patterns distorted by the Coriolis resonance between the  $\nu_2 = 1$  and  $\nu_5 = 1$  levels are essentially the same. Differences can only be found in details corresponding to shifted positions of the level crossings with respect to the  $J$  rotational quantum number. These level crossings are due to the  $\alpha$ -resonances and the weak Coriolis resonance between the  $\nu_5 = 1$  and  $\nu_3 = 2$  levels. The overtone band  $2\nu_3$ , which is the only one with significantly changed band origin (from  $1409.7 \text{ cm}^{-1}$  in the 1337 species to  $1421.3 \text{ cm}^{-1}$  in the 1335 species), is too weak to be seen in the short path length spectrum 35-4 in Fig. 1.

The prominent  $Q$ -branches of the  $\nu_5$  band can be used as a straightforward starting point for assigning this perpendicular band. On the high-wavenumber ( $\Delta K = +1$ ) side of the band the  $^rQ_K$ -branches can be followed up to  $K=12$ . The  $^pQ_K$ -branches on the low-wavenumber side of the  $\nu_5$

band can be easily followed only to  $K=6$ . For  $K=7$  and  $8$  the  ${}^pQ_K$ -branches become more extended over several tens of  $\text{cm}^{-1}$  due to the approaching Coriolis resonance, as was in detail described in the previous analysis [2]. Because of this resonance, the  ${}^pQ_K$ -branches with  $K \geq 9$  have strongly depleted intensities.

In several places of the spectrum, the regular patterns of the  $Q_K$ -branches have visible gaps, which indicate the presence of local resonances. Such effects can be clearly seen in the overview spectrum, for example in the  ${}^pQ_3$  branch (Coriolis resonance with the  $v_3 = 2$  level). In the  $v_5$  band we have assigned more than 3200 rovibrational transitions up to  $J/K = 70/15$ .

The strongest interaction in the studied polyad, the first-order Coriolis resonance between the  $v_2 = 1$  and  $v_5 = 1$  levels, affects all branches of the  $v_2$  band in a very illustrative way. That is why the  $Q$ -branch region of this parallel band (around  $1449.5 \text{ cm}^{-1}$ ) is not compact as appears in unperturbed parallel bands, but widely spread, as shown in Fig. 2. With growing  $K$  up to the crossing, the  ${}^qQ_K$  branches become more and more degraded to lower wavenumbers. Starting from  $K=9$ , which is the first  $K$  value after the resonant crossing, the  ${}^qQ_K$  branches become degraded towards higher wavenumbers. The intensities of these  ${}^qQ_K$ -branches slowly decrease with  $K$  with and reveal a regular spin statistical pattern. This confirms the fact, that intensities of  ${}^qQ_K$ -branches of a parallel band are not affected by the Coriolis resonance [8].

At low values of the  $J$  quantum number the typical patterns of  $P$ - and  $R$ -branches of a parallel band can be easily followed (see also Fig. 2) and used as a reliable starting point of assignments. At higher values of  $J$ , however, this regular structure starts to be heavily perturbed by the Coriolis resonance as shown in Fig. 3. For assignments of these strongly perturbed transitions we took the great advantage of the interactive Loomis-Wood graphical program with lower state combination difference checking (LW-LSCD) [9], which provided reliable assignments of rotational quantum numbers. In the  $v_2$  band we have assigned more than 1600 rovibrational transitions up to  $J/K = 66/14$ .

The LW-LSCD program was also very helpful for the assignment of the weak  $2v_3$  overtone band. Starting with a reasonable prediction of the upper state constants, we obtained from the longer path length spectrum 35-5 clearly visible patterns in the Loomis-Wood diagrams. The correct assignments of the  $J/K$  quantum numbers were found to be unambiguous by lower state combination difference checking. The assignments in the overtone  $2v_3$  band were extended up to  $J/K = 52/9$ , yielding more than 880 transitions.

With the preliminary assignment and the fit of molecular parameters we were able to calculate the rovibrational energies and estimate the positions of the resonant crossings due to the weaker Coriolis resonance between the  $v_3 = 2$  and  $v_5 = 1$  levels and the two  $\alpha$ -resonances

between the  $v_5 = 1$  level and the two nondegenerate  $v_2 = 1$  and  $v_3 = 2$  levels. The resonances are clearly shown in the reduced energy diagram in Fig. 4. On its left hand side, the relative positions of the lowest  $K$  levels are shown with indication of the mentioned resonances. On the right hand side the  $J$ -progressions of all these levels are shown in order to illustrate the positions of local crossings in dependence of  $J$ . In the reduced energy plot the purely  $J$ -dependent part of the rotational energy (as calculated from the ground state constants) is subtracted from the total vibration-rotation energy  $E_{vr}$

$$E_{red} = E_{vr}(J, k, l) - B_0 J(J+1) + D_J^0 J^2(J+1)^2 - H_J^0 J^3(J+1)^3.$$

Therefore, the slopes of the  $J$ -series correspond in the first approximation to the difference  $\Delta B_v = B_v - B_0$ . It is noted, that owing to the small value of  $\Delta B_5 \approx 0.32 \times 10^{-3} \text{ cm}^{-1}$  almost horizontal  $J$ -series appear in the reduced energy plot for those levels in the  $v_5 = 1$  state that are not perturbed by resonance interactions. There are, on the other hand, large differences among the  $B$  constants of the vibrational levels in the polyad ( $B_2 - B_5 \approx -1.88 \times 10^{-3} \text{ cm}^{-1}$  and  $B_{33} - B_5 \approx -7.62 \times 10^{-3} \text{ cm}^{-1}$ ). These differences bridge the energy gaps between interacting levels and repeatedly cause the occurrence of resonant crossings as shown in Fig. 4. These crossings due to the second-order Coriolis interaction ( $\Delta k = \pm 1, \Delta l = \pm 1$ ) can be located in the reduced energy plot in the succession of level pairs  $(v_3 = 2, K) - (v_5 = 1^{-1}, K-1)$  with  $K = 3 - 6$ , occurring between  $J = 9/10, 36/37, 50/51$ , and  $61/62$ , respectively. These crossings are also clearly visible in the survey spectrum in Fig. 1 as wide gaps in the patterns of the  ${}^p Q_{3-}, {}^p Q_{4-}$ , and  ${}^p Q_{5-}$ -branches of the  $v_5$  band.

In addition to these Coriolis resonances, there are also local  $\alpha$ -resonances ( $\Delta k = \pm 2, \Delta l = \mp 1$ ) between the  $v_5 = 1$  level and the two nondegenerate  $v_2 = 1$  and  $v_3 = 2$  levels. These resonances occur between the level pairs  $(v_5 = 1^{+1}, K) - (v_2 = 1, K+2)$  with  $K = 5$  and  $6$  (at  $J = 21/22$  and  $50/51$ , respectively) and the level pair  $(v_5 = 1^{+1}, K) - (v_3 = 2, K+2)$  with  $K = 1$ . Since the levels  $(v_5 = 1^{+1}, K=1)$  as well as  $(v_3 = 2, K=3)$  are split into two resolvable  $A_+ - A_-$  components, the respective local resonances occur at different  $J$  values, in particular between  $J = 26/27$  and  $30/31$ , for  $A_+$  and  $A_-$ , respectively. Details of resonant crossings occurring between the levels with the lowest values of  $K$  are shown in Fig. 5.

The above-mentioned  $\alpha$ -resonances induce series of perturbation-allowed transitions with selection rules  $\Delta k = -2, \Delta l = +1$  in the  $v_5$  band and  $\Delta k = +3, \Delta l = 0$  in the  $v_2$  and  $2v_3$  bands. A detail of the spectrum illustrating the  ${}^r Q_{4-}$ -branch of the  $v_5$  band, perturbed by the  $\alpha$ -resonance crossing at  $J = 21/22$ , accompanied by the perturbation-allowed branch  ${}^t Q_{4-}$ -branch (formally

belonging to the  $\nu_2$  band) is shown in Fig. 6. As already stated, the wavenumbers of PA transitions combined with those of normally allowed transitions provide energy spacings between pairs of levels of the vibrational ground state differing in the  $K$  quantum number by 3 ( $K = 0 - 3, 4 - 7, \text{ and } 5 - 8$ ). These differences allow the independent determination of the  $A_0$ ,  $D_K^0$ , and in principle also  $H_K^0$  constants.

#### 4. Description of the rotational spectra

The rotational spectra recorded in the present study cover the ranges of  $J$  values 6-13 and 19-24. In the lower frequency range we provide most important data around the Coriolis crossing between  $\nu_3 = 2$  and  $\nu_5 = 1$  at  $J = 9/10$ , in the higher frequency range around the  $\alpha$ -resonance crossing between  $\nu_2 = 1$  and  $\nu_5 = 1$  at  $J = 21/22$  and also approaching the other  $\alpha$ -resonance crossing between  $\nu_3 = 2$  and  $\nu_5 = 1$  at  $J = 26/27$ . All these data contribute significantly to an accurate determination of the corresponding interaction terms as well as the ground state axial rotational and centrifugal distortion constants. We were able to record and assign rotational transitions with  $K$  up to 14 in all studied vibrational levels. Since the levels ( $\nu_5 = 1, k = \pm 2, l = \mp 1$ ) and ( $\nu_3 = 2, k = \pm 3$ ) were split into  $A_+-A_-$  components by rovibrational interactions, we recorded resolvable splittings of the rotational transitions of the  $\nu_5 = 1$  state in the range of  $J = 19-22$  and  $J = 19-24$  in the  $\nu_3 = 2$  state. The  $A_+-A_-$  components of the rotational transitions in the  $\nu_2 = 1$  level were not resolved.

Due to the large value of the quadrupole moment of the chlorine nucleus and its interaction with the gradient of the electric field in its vicinity, significant quadrupole hyperfine splittings have been observed. In order to merge rotational data into a simultaneous fit with rovibrational wavenumbers, we first calculated purely rotational (hyperfine-free) frequencies from the resolved hyperfine structures. With the spin of the chlorine nucleus  $I = \frac{3}{2}$ , the total angular momentum  $F$  acquires the values

$$F = |J - I|, \dots, |J + I| = J - \frac{3}{2}, J - \frac{1}{2}, J + \frac{1}{2}, J + \frac{3}{2}$$

and therefore all levels with  $J \geq 2$  are split into four hyperfine components. For a symmetric top molecule with the quadrupolar nucleus on the symmetry axis the energies of the components can be calculated as diagonal elements of the electric-quadrupole Hamiltonian

$$\langle J, K, F | H_{hfs} | J, K, F \rangle = eQq \left[ \frac{3K^2}{J(J+1)} - 1 \right] \left[ \frac{\frac{3}{4} C(C+1) - I(I+1)J(J+1)}{2I(2I-1)(2J-1)(2J+3)} \right]$$

where  $C = F(F+1) - J(J+1) - I(I+1)$  is the Casimir function and the electric-quadrupole coupling constant  $eQq$  is the product of the proton charge  $e$ , the nuclear quadrupole  $Q$ , and  $q$

which is the expectation value of the space-fixed  $zz$ -component of the electric field gradient tensor averaged over the rotational motion.

The splittings of the strongest  $\Delta F = +1$  hyperfine components of rotational transitions into quadruplets were resolved for  $J$  up to 10 and for  $K \geq 4$ . For lower values of  $K$  the quadruplets collapse first into doublets and then further into a single line with unresolved hyperfine structure. The typical situation for transitions  $J = 8 \leftarrow 7$  in the  $v_3 = 2$  vibrational state is shown in Fig. 7. For values of  $J$  above 10 only doublets, collapsing into single lines for low  $K$ , were observed. From hyperfine multiplets with resolved splittings the purely rotation frequencies were calculated using a value of  $eQq = -74.8$  MHz taken from a previous microwave study [10]. We have estimated the accuracy of the frequency determination of individual resolved lines, after subtracting the baseline signal and fitting a profile function to each spectral peak, to be better than 25 kHz. This is also assumed to be the accuracy of purely rotational frequencies calculated from the resolved quadruplets. When the hyperfine quadruplets had collapsed into doublets and single lines, the positions of individual hyperfine components within the line envelope were calculated from the maximum of the peak, assuming that it appeared at the frequency of an intensity-weighted average of the overlapped lines. The accuracy of the purely rotational frequencies calculated from partially resolved or unresolved hyperfine structures was estimated to be slightly poorer, but better than 30 kHz.

## 5. Results and discussion

The effective vibration-rotation Hamiltonian used in the present analysis is essentially the same as in the previous study of the 1337 species [2]. The matrix elements employed in the present work are summarized in the Appendix B. In the weighted least squares fit the experimental data were given weights proportional to the inverse square of their estimated experimental uncertainty. We have refined together 51 upper state parameters and all vibrational ground state constants up to the sextic centrifugal distortion terms. The fitted parameters of the effective vibration-rotation Hamiltonian are listed in Tables 1 and 2.

Our strategy of fitting the axial ground state constants together with the upper state parameters improved reproduction of all data in the excited vibrational states considerably and allowed even the determination of the  $H_K^0$  constant with apparently excellent precision. The statistical error of the  $A_0$  constant was improved by a factor of more than 40 with respect to the previous work [1] and the errors of the centrifugal distortion constants, determined here experimentally for the first time, are of the order of 0.1 and 0.5 percent of the values of  $D_K^0$  and  $H_K^0$ , respectively.

Fitting of the ground state rotational frequencies together with the upper state data proves the consistency of the whole analysis. The standard deviation of reproduction of the ground state data thereby increases only to 7.4 kHz from that of 6.3 kHz, when the ground state rotational frequencies were fitted alone. Also the values of the non-axial constants of the ground vibrational state stay within their 3- $\sigma$  error intervals with respect to those determined from the fit of only the ground state data. The values from the joint fit are also in excellent agreement with those of the previous study [1].

The ranges of assigned rotational quantum numbers in the ground and the excited states in individual IR bands and for the MMW measurements used in the fit, estimated accuracies of strong unsaturated and isolated lines, and standard deviations of reproduction are summarized in Table 3. In the analysis we practically achieved a quantitative reproduction of all IR and MMW data with respect to the estimated experimental accuracies.

In order to maintain a good reproduction of low- $K$  transitions in both  $v_5 = 1$  and  $v_3 = 2$  states, we had to refine the  $q_{12}$  term, despite its rather high correlation with the leading term  $\alpha_{25}^{BB}$  of the  $\alpha$ -resonance between  $v_5 = 1$  and  $v_2 = 1$ . Only with inclusion of  $q_{12}$  we were able to avoid rapidly increasing errors of reproduction in the  ${}^rQ_0$ -branch of the  $v_5$  band and the low- $K$  rotational transitions in the  $v_5 = 1$  vibrational state. For the same reason, we also had to include one of the higher order terms of the Coriolis ( $B\zeta_{335}^{(2)}$ ) or the  $\alpha$ -resonance ( $\alpha_{335}^K$ ) between the  $v_5 = 1$  and  $v_3 = 2$  states. Fitting of  $\alpha_{335}^K$  led only to a slightly better overall reproduction of data, but at the price of considerably increased correlations among many of the interaction parameters. On the other hand, refining  $B\zeta_{335}^{(2)}$  instead, slightly worsened the data reproduction but removed the correlations and therefore we gave preference to the latter interaction model in the final data fit. The necessity to include such higher-order interaction terms in order to correctly fit the data associated with the low- $K$  states indicates that at the achieved level of data accuracy, effects due to additional perturbations by levels belonging to other polyads may be of importance. Attempts to replace these interaction terms by the  $\tau_K$  constant led to undetermined and highly correlated values and thus  $\tau_K$  was constrained to zero in the fit.

All these reasons may also be responsible for the surprisingly large value of the  $H_K^0$  constant (cf. Table 1), which is more than twice the value determined in the analysis of the same polyad of the 1337 [2] species and also the *ab initio* value [Ref. 11]. Therefore the present  $H_K^0$  parameter has to be considered as rather effective and still depending on the fit of the various  $\alpha$ -resonance crossings. The reason for the difference between the two isotopic species of methyl

chloride, the previous case of 1337 [2] and the present one of 1335 is supposedly the following: here the  $\alpha$ -resonance between the  $v_3 = 2$  and  $v_5 = 1$  levels occurs for low- $K$  levels split into  $A_+$ - $A_-$  ( $A_1/A_2$ ) symmetry components. For these the neglected Coriolis couplings with levels outside the currently studied polyad may play an important role because only one of these levels is influenced by that interaction. This may lead to effective rather than true values of some parameters. Such an influence was also demonstrated in a related study of the methyl fluoride isotopic species [12,13]. There only inclusion also of Coriolis couplings linking the  $v_2 = 1 / v_5 = 1$  dyad with the  $v_3 = 1$  and  $v_6 = 1$  fundamental levels allowed a quantitative fitting of the low- $K$  levels. We furthermore point out that in the 1337 species of methyl chloride the  $\alpha$ -resonance affected only levels with E rotational symmetry [2].

Additional differences between observed and calculated wavenumbers occur for some high- $K$  values. These can be attributed to higher order resonances with levels not belonging to the studied  $v_2 = 1 / v_5 = 1 / v_3 = 2$  vibrational states, namely the  $v_6 = 1$  level and the next higher combination  $v_3 = v_6 = 1$  vibrational state, which is estimated to lie around  $1720 \text{ cm}^{-1}$ . The shifted levels and their interacting counterparts are the following

$$(v_2 = 1, K = 12) - (v_3 = v_6 = 1, l_6 = -1, K = 8) / \Delta k = \pm 4, \Delta l = \pm 1 \text{ interaction}$$

$$(v_5 = 1, l_5 = -1, K = 11) - (v_6 = 1, l_6 = -1, K = 14) / \Delta k = \pm 3, \Sigma(\Delta l) = 0 \text{ interaction}$$

$$(v_5 = 1, l_5 = -1, K = 13) - (v_3 = v_6 = 1, l_6 = -1, K = 10) / \Delta k = \pm 3, \Sigma(\Delta l) = 0 \text{ interaction.}$$

Data whose deviations of reproduction due to these resonances exceeded the assumed experimental uncertainty were given zero weights in the fits. An extension of the present analysis, however, was not intended in the present study, which was focused on describing the interactions within this polyad and the use of PA transitions for an accurate determination of axial ground state constants.

Moreover, one of the  $\Delta k = \pm 4, \Delta l = \pm 1$  resonances, connecting the pair of levels  $(v_5 = 1, l_5 = -1, K = 1) - (v_2 = 1, K = 5)$ , with a level crossing occurring between  $J = 54/55$  (see Fig. 4) was found within the studied polyad. Transitions assigned in both states and on both sides of the crossing, made it possible to determine the interaction constant of the coupling matrix element given in the Appendix (B9).

The sign of the  $f_{42}$  term responsible for the splitting of the  $k = \pm 2, l = \mp 1$  levels in  $v_5 = 1$  was determined in the same way as in the 1337 species. While the reproduction of data was more or less the same for both relative positions possible for the  $A_+$ - $A_-$  levels, the statistical error of the  $f_{42}$  term and its correlation with other interaction parameters (especially with  $q_{22}$ ) were

significantly smaller when  $A_-$  laid above  $A_+$ . Also the value of  $f_{42}$  of 1335 was found to be in good agreement with that of the 1337 species.

## **6. Conclusion**

The present analysis of FTIR and subterahertz spectra pertaining to the  $v_2 = 1$ ,  $v_5 = 1$ , and  $v_3 = 2$  levels of  $^{13}\text{CH}_3\ ^{35}\text{Cl}$  has provided a consistent and accurate description of this polyad. By inclusion of PA transitions induced by the  $\alpha$ -resonance between the  $v_2 = 1$  and  $v_5 = 1$  vibrational states, of local upper state effects provoked by the  $\alpha$ -resonance between the  $v_3 = 2$  and  $v_5 = 1$  vibrational states, and of ground state rotational frequencies, we were able to determine accurately the axial ground state constants  $A_0$  and  $D_K^0$ , and with due reservation  $H_K^0$ . Refinement of these ground state parameters in the fit improved considerably the description of all resonances within the studied system.

## **Acknowledgements**

This work was supported by the Grant Agency of the Czech Republic (project AA400400504), the Academy of Sciences of the Czech Republic (project 1ET400400410), and the Ministry of Education, Youth and Sports of the Czech Republic (research program LC06071). Support from Université de Lille I through the PAST contract awarded to one of the authors (P.P.) is gratefully acknowledged. H.B. and M.L. thank the Fonds der Chemie for support. We also wish to thank the authors of the ground state rotational study [5] for kindly providing their data prior to publication.

## Appendix A. Supplementary data

Supplementary data for this article are available in the online version at doi:

## Appendix B.

The Hamiltonian employed in the calculations of vibration-rotation levels had the following form. The diagonal matrix elements up to sixth order were taken as

$$\begin{aligned}
 E_{vr}^0(J, k, l) = & E_v + B_v J(J+1) + (A_v - B_v) k^2 - D_J^v J^2 (J+1)^2 - D_{JK}^v J(J+1) k^2 - D_K^v k^4 + \\
 & + H_J^v J^3 (J+1)^3 + H_{JK}^v J^2 (J+1)^2 k^2 + H_{KJ}^v J(J+1) k^4 + H_K^v k^6 + \\
 & + \left[ -2A\zeta_v + \eta_J^v J(J+1) + \eta_K^v k^2 + \tau_J^v J^2 (J+1)^2 + \tau_{JK}^v J(J+1) k^2 + \tau_K^v k^4 \right] kl.
 \end{aligned} \tag{B1}$$

Obviously, the third line of equation (A1) is valid only for the degenerate vibrational level  $v_5 = 1$  with  $l = \pm 1$ . Within this vibrational level the following  $l$ -type operators were taken into account

$$\langle v_i^l; J, k | (\mathbf{H}_{22} + \mathbf{H}_{24}) / hc | v_i^{l\mp 2}; J, k \pm 1 \rangle = 2 q_{12} (2k \pm 1) F_1^\pm(J, k) \tag{B2}$$

$$\begin{aligned}
 \langle v_i^l; J, k | (\mathbf{H}_{22} + \mathbf{H}_{24}) / hc | v_i^{l\pm 2}; J, k \pm 2 \rangle = \\
 = 2 \left\{ q_{22} + q_{22}^J J(J+1) + q_{22}^K [k^2 + (k \pm 2)^2] \right\} F_2^\pm(J, k)
 \end{aligned} \tag{B3}$$

$$\langle v_i^l; J, k | \mathbf{H}_{24} / hc | v_i^{l\mp 2}; J, k \pm 4 \rangle = 2 f_{42} F_4^\pm(J, k) \tag{B4}$$

The Coriolis interaction between  $v_2 = 1$  and  $v_5 = 1$  was accounted for by the matrix elements (with the  $k$ -dependent terms omitted)

$$\begin{aligned}
 \langle v_2 = 1, v_5 = 0^0; J, k | (\mathbf{H}_{21} + \mathbf{H}_{23} + \mathbf{H}_{25}) / hc | v_2 = 0, v_5 = 1^{\pm 1}; J, k \pm 1 \rangle = \\
 = \pm \sqrt{2} \left\{ B\zeta_{25}^y \Omega_{25} + \zeta_{25}^J J(J+1) + \zeta_{25}^{JJ} J^2 (J+1)^2 \right\} F_1^\pm(J, k)
 \end{aligned} \tag{B5}$$

The matrix element of the Coriolis interaction between  $v_3 = 2$  and  $v_5 = 1$ , which is a higher-order analogue of that in equation (A5), was supplemented by an additional  $k$ -dependent term

$$\begin{aligned}
 \langle v_3 = 2, v_5 = 0^0; J, k | (\mathbf{H}_{31} + \mathbf{H}_{33} + \mathbf{H}_{35}) / hc | v_3 = 0, v_5 = 1^{\pm 1}; J, k \pm 1 \rangle = \\
 = \sqrt{2} \left\{ \pm \left[ B\zeta_{335}^y + \zeta_{335}^J J(J+1) \right] + B\zeta_{335}^{(2)} (2k \pm 1) \right\} F_1^\pm(J, k)
 \end{aligned} \tag{B6}$$

The matrix element of the  $\alpha$ -resonance between  $v_2 = 1$  and  $v_5 = 1$  had the form

$$\begin{aligned} & \langle v_2 = 1, v_5 = 0^0; J, k | (\mathbf{H}_{22} + \mathbf{H}_{24}) / hc | v_2 = 0, v_5 = 1^{\mp 1}; J, k \pm 2 \rangle = \\ & = 1 / (2\sqrt{2}) \left\{ \alpha_{25}^{BB} + \alpha_{25}^{BB,J} J(J+1) + \alpha_{25}^{BB,K} [k^2 + (k \pm 2)^2] \right\} F_2^{\pm}(J, k) \end{aligned} \quad (\text{B7})$$

and the  $\alpha$ -resonance between  $v_3 = 2$  and  $v_5 = 1$  had analogous higher-order matrix elements

$$\begin{aligned} & \langle v_3 = 2, v_5 = 0^0; J, k | (\mathbf{H}_{32} + \mathbf{H}_{34}) / hc | v_3 = 0, v_5 = 1^{\pm 1}; J, k \pm 1 \rangle = \\ & = 1 / (2\sqrt{2}) \left\{ \alpha_{335}^{BB} + \alpha_{335}^{BB,J} J(J+1) + \alpha_{335}^{BB,K} [k^2 + (k \pm 2)^2] \right\} F_2^{\pm}(J, k) \end{aligned} \quad (\text{B8})$$

The matrix element of the  $\Delta k = \pm 4, \Delta l = \pm 1$  interaction has a general form [13]

$$\langle v_5^{\mp 1}; J, k | \mathbf{H}_{24} / hc | v_2; J, k \pm 4 \rangle = \sqrt{2} q_{42}^{25} F_4^{\pm}(J, k). \quad (\text{B9})$$

The notation for the rotational part of the matrix elements was taken conventionally as

$$F_n^{\pm}(J, k) = \prod_{i=1}^n [J(J+1) - (k \pm i \mp 1)(k \pm i)]^{1/2}. \quad (\text{B10})$$

## References

- [1] M. Litz, H. Bürger, L. Féjard, F.L. Constantin, L. Margulès, J. Demaison, J. Mol. Spectrosc. 219 (2003) 238-247.
- [2] F. L. Constantin, J. Demaison, L. Féjard, M. Litz, H. Bürger, P. Pracna, Mol. Phys. 102 (2004) 1717-1730.
- [3] J.L. Duncan, A. Allan, J. Mol. Spectrosc. 25 (1968) 224-239.
- [4] G.M. Black, M.M. Law, J. Mol. Spectrosc. 205 (2001) 280-285.
- [5] L. Stříteská, M. Šimečková, P. Kania, Š. Urban (*in preparation*)
- [6] A. Nikitin, L. Féjard, J.P. Champion, H. Bürger, M. Litz, J.-M. Colmont, B. Bakri, J.Mol.Spectrosc. 221 (2003) 199-212.
- [7] A. Nikitin, J.P. Champion, H. Bürger, J. Mol. Spectrosc. 230 (2005) 174-184.
- [8] C. Dilauro, I.M. Mills, J. Mol. Spectrosc. 21 (1966) 386-413.
- [9] Š. Urban, J. Behrend, P. Pracna, J. Mol. Struct. 690 (2004) 105-114.
- [10] M. Imachi, Y. Tanaka, E. Hirota, J. Mol. Spectrosc. 63 (1976) 224-280.
- [11] W. Schneider, W. Thiel, Chem. Phys. 159 (1992) 49-66.
- [12] D. Papoušek, J. Demaison, J., G. Wlodarczak, P. Pracna, S. Klee, M. Winnewisser, J. Mol. Spectrosc. 192 (1994) 220-227.
- [13] D. Papoušek, M. Winnewisser, S. Klee, L. Demaison, P. Pracna, J. Mol. Spectrosc. 196 (1999) 319-323.

### Table Captions

Table 1

Vibrational energies, rotational and centrifugal distortion constants (in units of  $\text{cm}^{-1}$ ) of the vibrational ground state and the  $v_3 = 2$ ,  $v_2 = 1$ , and  $v_5 = 1$ , upper states of  $^{13}\text{CH}_3\ ^{35}\text{Cl}$ . Numbers in parentheses are standard deviations in units of the last digit quoted.

	$v = 0$	$v_3 = 2$	$v_2 = 1$	$v_5 = 1$
$E$	0.0	1421.342 386 (17)	1349.329 360 (14)	1449.585 512 (10)
$B$	0.426 834 731 (5)	0.419 532 647 (57)	0.425 268 099 (10)	0.427 151 491 (79)
$A$	5.205 746 9 (55)	5.189 230 4 (61)	5.228 420 3 (55)	5.159 956 7 (51)
$D_J \times 10^{-7}$	5.656 58 (8)	5.613 46 (22)	5.672 99 (15)	5.745 48 (14)
$D_{JK} \times 10^{-6}$	6.308 46 (17)	6.261 97 (20)	6.348 61 (34)	6.225 03 (17)
$D_K \times 10^{-5}$	8.440 4 (84)	8.272 5 (117)	8.755 4 (85)	8.240 6 (84)
$H_J \times 10^{-13}$	-3.115 (50)	-3.880 (87)	-3.447 (62)	-2.861 (51)
$H_{JK} \times 10^{-12}$	9.865 (121)	15.770 (178)	18.631 (194)	2.724 (145)
$H_{KJ} \times 10^{-10}$	3.106 (16)	3.190 (7)	4.554 (32)	4.697 (7)
$H_K \times 10^{-9}$	8.527 (39)	5.677 (725)	8.113 (90)	8.321 (33)

Table 2

Coriolis and  $l$ -type parameters within the  $v_5 = 1$  level and parameters of Coriolis and  $\alpha$ -resonances of the  $v_5 = 1$  state with the  $v_2 = 1$  and  $v_3 = 2$  levels of  $^{13}\text{CH}_3\ ^{35}\text{Cl}$  (in units of  $\text{cm}^{-1}$ ).

Numbers in parentheses are standard deviations in units of the last digit quoted.

$v_5 = 1$		Interaction terms	
$A\zeta_5$	- 1.280 822 5 (53)	$B\zeta_{25}^y \Omega_{25}$	- 0.243 841 77 (17)
$\eta_J \times 10^{-4}$	- 0.156 90 (105)	$\zeta_{25}^J \times 10^{-7}$	6.781 2 (141)
$\eta_K \times 10^{-4}$	- 1.428 1 (35)	$\zeta_{25}^{JJ} \times 10^{-12}$	1.512 (98)
$\tau_J \times 10^{-10}$	- 1.103 (11)	$B\zeta_{335}^y \times 10^{-2}$	1.577 0 (15)
$\tau_{JK} \times 10^{-8}$	7.250 (7)	$\zeta_{335}^J \times 10^{-6}$	- 3.647 7 (59)
		$B\zeta_{335}^{(2)} \times 10^{-3}$	- 2.659 9 (32)
$q_{22} \times 10^{-4}$	- 1.000 87 (15)	$\alpha_{25}^{BB} \times 10^{-5}$	- 6.243 (559)
$q_{22}^J \times 10^{-9}$	- 1.976 8 (65)	$\alpha_{25}^{BB,K} \times 10^{-7}$	1.093 (36)
$q_{12} \times 10^{-4}$	6.195 (238)	$\alpha_{335}^{BB} \times 10^{-5}$	2.433 (61)
$f_{42} \times 10^{-10}$	- 5.589 0 (231)	$\alpha_{335}^{BB,J} \times 10^{-9}$	- 3.007 (95)
		$\alpha_{335}^{BB,K} \times 10^{-7}$	5.574 (158)
		$f_{41}^{25} \times 10^{-9}$	3.605 (184)

Table 3

Summary of experimental data of  $^{13}\text{CH}_3\ ^{35}\text{Cl}$  used in the analysis with their ranges of rotational quantum numbers, accuracy, and standard deviations of reproduction.

	Range of J/K	No. of data <sup>a</sup>	Estimated accuracy <sup>b</sup>	Standard deviation <sup>b</sup>
$\nu_2$ IR	66 / 14	1632 / 1571		1.90
$\nu_5$ IR	70 / 15	3205 / 3057	2.0	1.92
$2\nu_3$ IR	52 / 9	884 / 756		1.96
PA <sup>c</sup> IR	54 / 0-7	79 / 77		2.07
$\nu_2 = 1$ MMW	6-23 / 13	126 / 113		55
$\nu_5 = 1$ MMW	6-23 / 15	270 / 259	25	70
$\nu_3 = 2$ MMW	6-23 / 13	163 / 16320		39
$\nu = 0$ MMW	23 / 15	86 / 77	50	7.4

<sup>a</sup>Total number of data / number of data with nonzero weights.

<sup>b</sup>In units of  $10^{-4}\text{ cm}^{-1}$  for IR data and kHz for MMW data.

<sup>c</sup>Perturbation-allowed transitions to levels  $\nu_2 = 1$ ,  $\nu_5 = 1$ , and  $\nu_3 = 2$ .

### Figure Captions

Fig. 1. Survey spectrum 35-4 of the region of the  $\nu_2$ ,  $\nu_5$ , and  $2\nu_3$  bands with the band origins and the  $Q_K$ -branches of the  $\nu_5$  band indicated. The  $2\nu_3$  overtone band is too weak to be discernible in this spectrum.

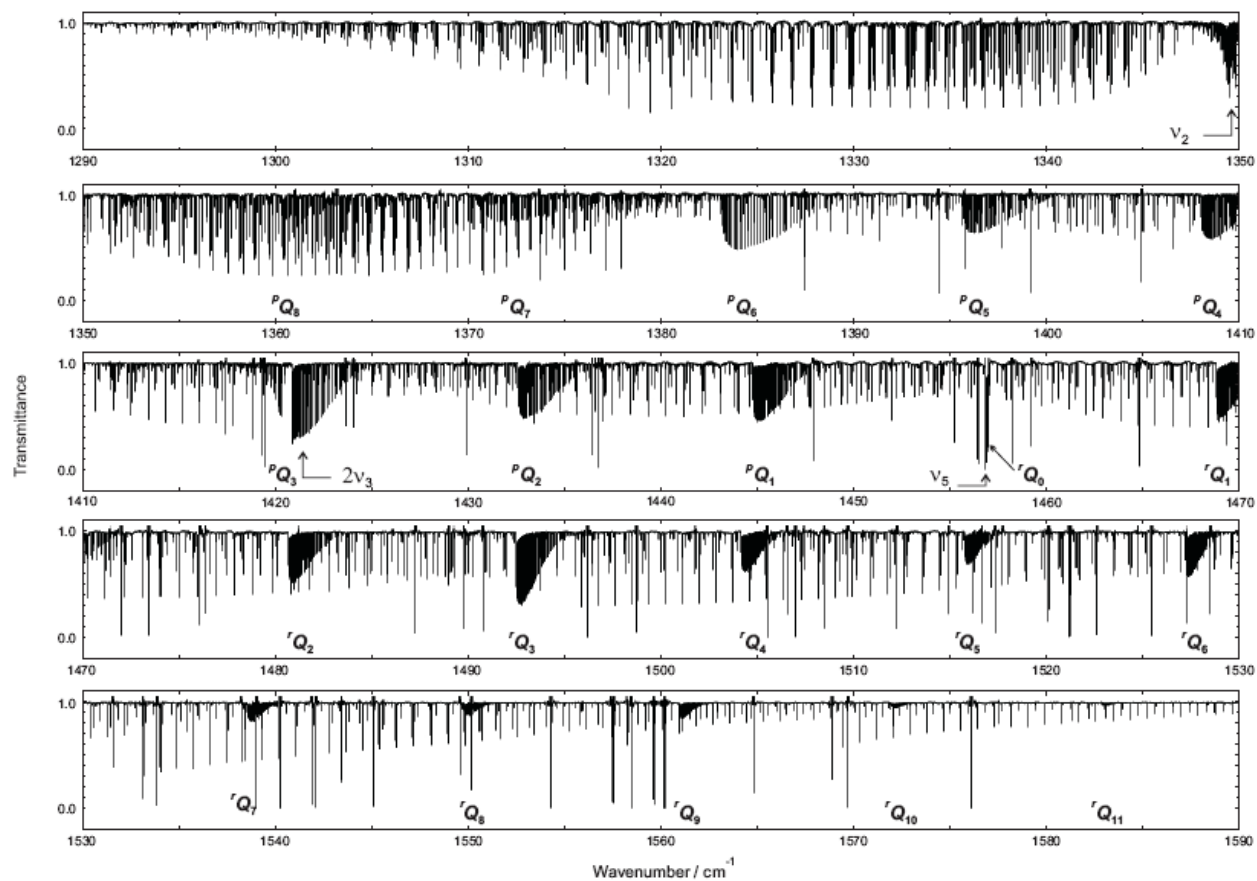


Fig. 2. Detail of the  $Q$ -branch region of the  $\nu_2$  band. The effect of the Coriolis resonance is demonstrated by the opposite direction of development of the  $Q$ -branches below ( $K \leq 8$ ) and above ( $K \geq 9$ ) the crossing. Also the some low- $J$   $K$ -clusters in the  $P$  and  $R$  branches of the  $\nu_2$  band are clearly visible.

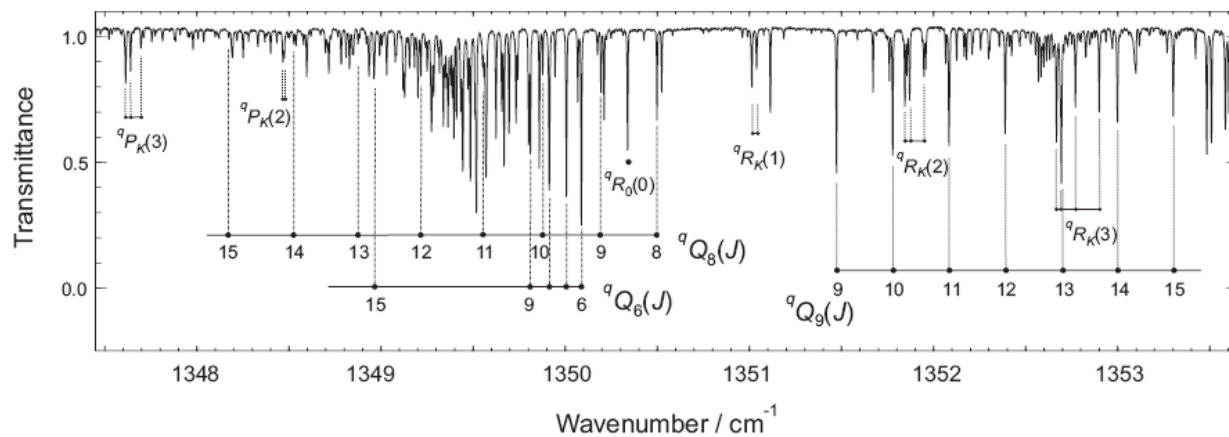


Fig. 3. Top trace: Details of the  $R$ -branch of the  $\nu_2$  band in the region of the assigned  ${}^P Q_8$ -branch. The effect of the Coriolis resonance on the  $K$  structure of the  ${}^Q R_K(10)$ -branch, discontinued between  $K = 8$  and  $9$ , is shown. The  ${}^Q R_K(J)$  labels given on top represent the starting points of the respective  $J$  clusters for  $J \geq 9$  with the value of  $K$  indicating the point of reversal of the  $K$  structure.

Bottom trace: Similar situation as in top trace for the  ${}^P Q_7/{}^Q R_K(20)$  region. Note that the  ${}^P Q_7$ - and, more pronouncedly,  ${}^P Q_8$ -branches show an increase of their  $J$  spacing due to the effective growth of  $\Delta B_5$  with increasing  $K$  in correspondence to the Coriolis resonance.

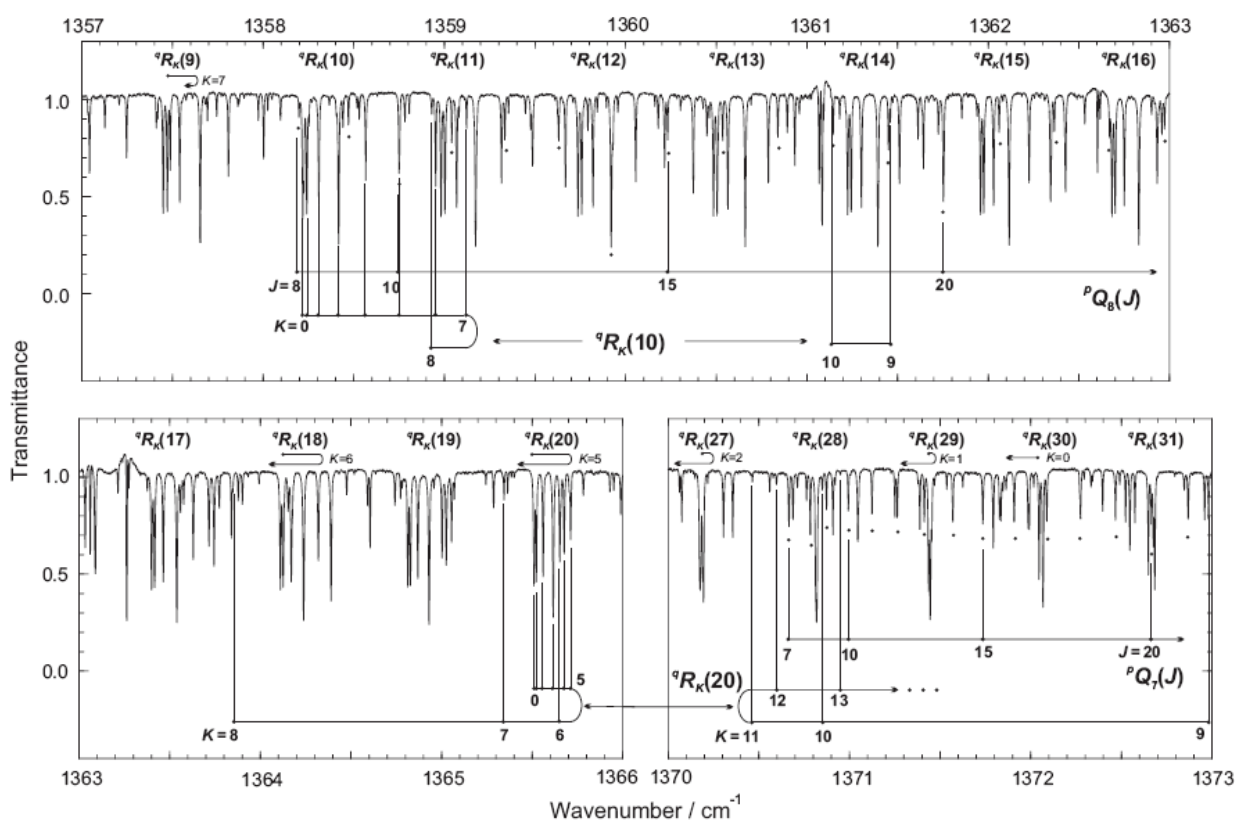


Fig. 4. Energy level diagram of the  $v_2 = 1$ ,  $v_5 = 1$ , and  $v_3 = 2$  levels with indication of major perturbations shown in the left part of the figure (Coriolis marked with full lines and  $\alpha$ -resonance with dashed lines). The  $J$ -dependences in the form of reduced energies are developed on the right side of the figure, indicating the positions of crossings ( $v_2 = 1 / v_5 = 1$  resonances in circles or ellipses and  $v_3 = 2 / v_5 = 1$  resonances in rectangles and thinner lines). Selected rovibrational energies (enclosed in the dotted frame), relevant for the interaction between the  $v_3 = 2$  and  $v_5 = 1$  levels, are shown further in detail in Fig. 5.

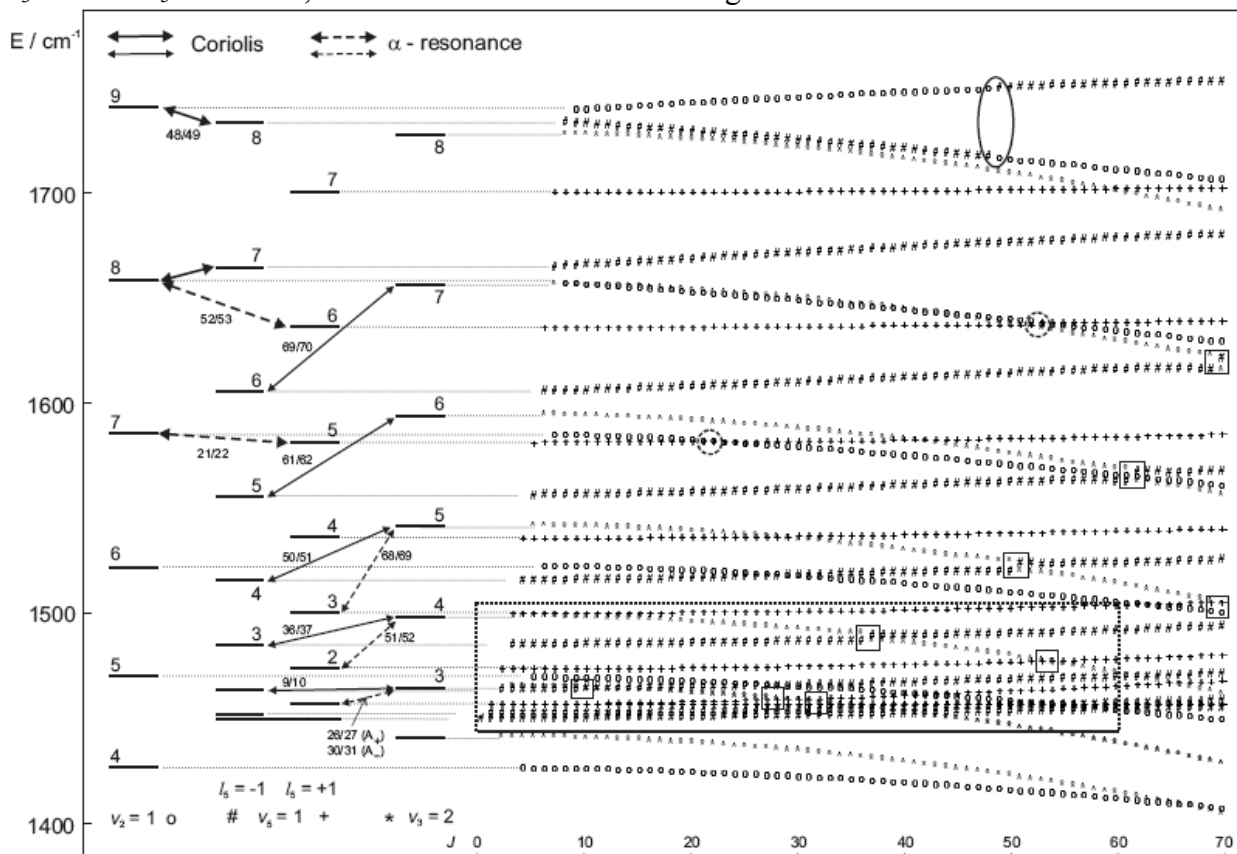


Fig. 5. A detail of the reduced energy level diagram (corresponding to the frame in Fig. 4.) showing resonant crossings between the levels with the lowest values of the  $K$  rotational quantum numbers.

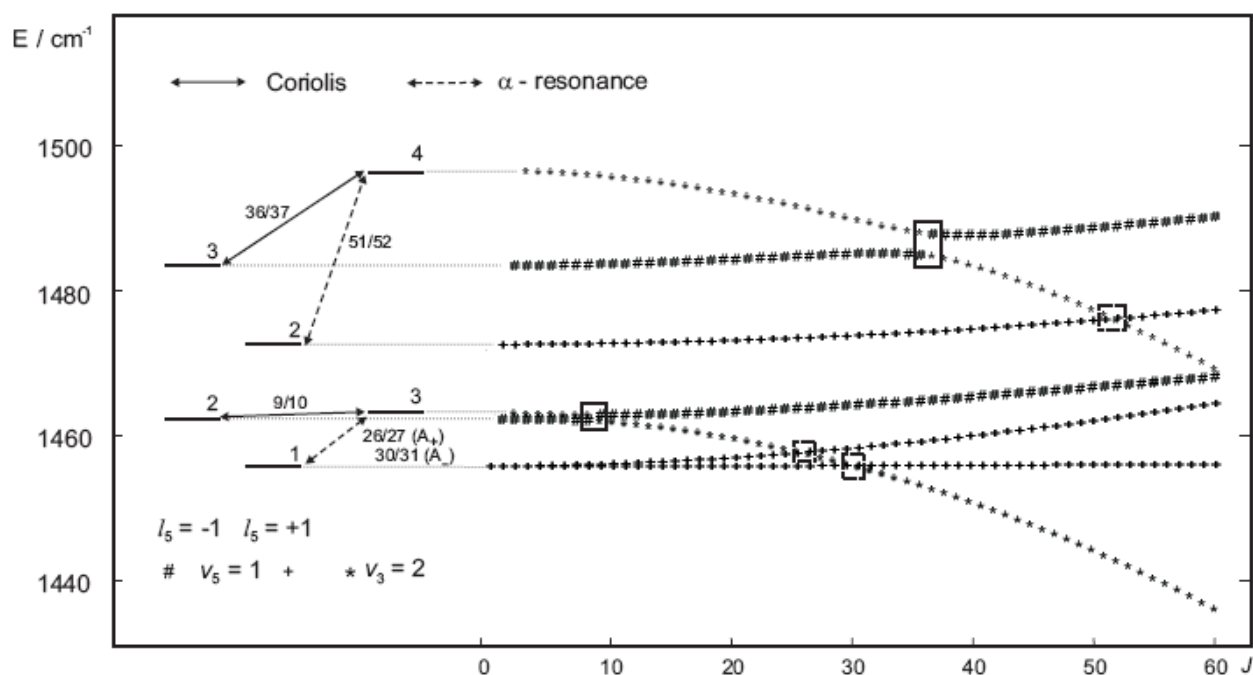


Fig. 6. Detail of the FT spectrum illustrating the effect of the  $\alpha$ -resonance in the  ${}^rQ_4$ -branch of the  $\nu_5$  band (upper assignment comb with values of  $J$ ) and the corresponding sequence of perturbation-allowed transitions  ${}^tQ_4$  (lower assignment comb), formally belonging to the  $\nu_2$  band.

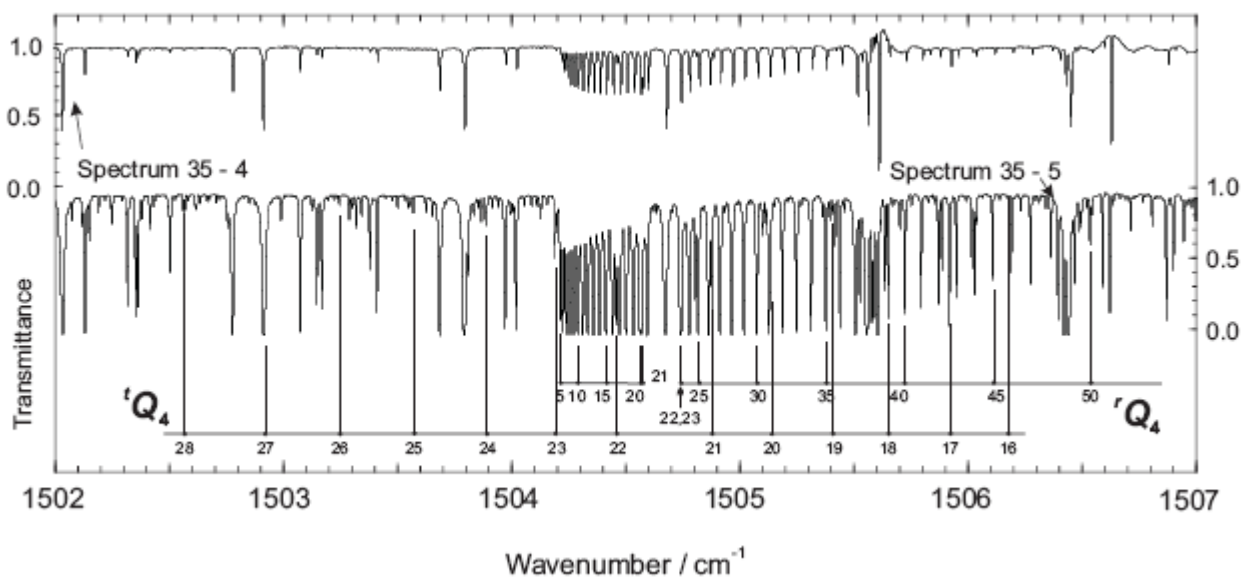


Fig. 7. Section of the rotational spectrum with transitions  $J = 8 \leftarrow 7$  in the  $v_3 = 2$  state showing details of their hyperfine splittings. The hyperfine components ( $\Delta F = +1$ ) are denoted with the lower state quantum numbers  $F$ . The  $K = 3$  and 4 transitions are shifted to considerably higher frequencies by the Coriolis resonance with the  $v_5 = 1$  vibrational state. Experimental conditions: sample pressure 4 Pa, accumulation time 0.6 s/point, BWO frequency modulation at 5 kHz with a depth of 400 kHz.

